Acta Cryst. (1999). B**55**, 563–572

Topological analysis of the electron density in hydrogen bonds

E. Espinosa,[a] M. Souhassou,[b] H. Lachekar[b] and C. Lecomte[b]*

[a]*Instituto de Ciencia de Materiales de Barcelona (CSIC), Campus de la UAB, 08193 Bellaterra (Barcelona), Spain, and* [b]*Laboratoire de Cristallographie et Modélisation des Matériaux Minéraux et Biologiques, UPRESA CNRS No. 7036, Université Henri Poincaré Nancy 1, Faculté des Sciences, BP 239, 54506 Vandoeuvre-lès-Nancy CEDEX, France. E-mail: lecomte@lcm3b.u-nancy.fr*

(*Received 30 October 1998; accepted 2 February 1999*)

Abstract

Topological analysis of the experimental electron density $\rho(\mathbf{r})$ in hydrogen-bonding regions has been carried out for a large number of organic compounds using different multipole models and techniques. Relevant systematic relationships between topological properties at the critical points and the usual geometric parameters are pointed out. Results involving X-ray data only and joint X-ray and neutron data, as well as special hydrogen bonding cases (symmetric, bifurcated, peptide bonds, *etc.*) are included and analysed in the same framework. A new classification of hydrogen bonds using the positive curvature of the electron density at the critical point $[\lambda_3(\mathbf{r}_{CP})]$ is proposed.

1. Introduction

Topological analysis of charge densities has been carried out on a large number of systems, involving single molecules, clusters or periodic arrangements. The theory of atoms in molecules (Bader, 1990, and references therein) was first applied to theoretical studies of molecules in the gas phase and in clusters; later, experimental and theoretical studies of periodic systems used the framework of this theory to study molecules in solids. Since topological analysis of the electron density $\rho(\mathbf{r})$ can be performed in periodic systems, intermolecular interactions represent a field of increasing interest. Experimental topological analysis of the electron density is frequently used to describe hydrogen-bond (HB) interactions, even if in most cases it corresponds to a description of only the observed topological properties, without any deeper analysis. On the other hand, theoretical studies [based on periodic Hartree–Fock *ab initio* SCF calculations (Dovesi *et al.*, 1995)] give, in general, a more detailed description of the HB interactions (Gatti *et al.*, 1994; Platts & Howard, 1996). Especially interesting is the study of urea by Gatti *et al.* (1994), which analyses the mechanisms associated with hydrogen-bond formation in the crystal.

In two recent papers (Espinosa *et al.*, 1998, 1999), we showed that relationships exist between the topology of $\rho(\mathbf{r})$ in the HB region and some energetic properties, such as the local potential (V^{CP}) and kinetic (G^{CP}) energy densities at the HB critical point (CP) (Bader, 1990), and the HB energy (E_{HB}) (through its proportionality to V^{CP}). In the first paper, we showed the exponential behaviour of G^{CP} and V^{CP} as a function of $d(H\cdots O)$, using Abramov (1997) functions and, in particular, the possibility of representing E_{HB} as a simple exponential function of $d(H\cdots O)$; this can be very useful in the estimation of E_{HB} when calculations and/or simulations of $H\cdots O$ interactions are involved. In the second paper, we discussed the relationships between the principal curvatures $(\lambda_1, \lambda_2, \lambda_3)$ of $\rho(\mathbf{r})$ at CPs and these energetic properties, leading to a new representation of the topological characteristics of $\rho(\mathbf{r})$ in terms of energetics and *vice versa*.

These papers were based on a selection of structural and topological data from accurate electron density studies involving $X-H\cdots O$ (X = C, N, O) hydrogen bonds which are discussed here in more detail; the aim of this paper is to identify other relevant systematic relationships between the topological properties of $\rho(\mathbf{r})$ and the usual geometrical parameters of HB interactions. Trends found by this analysis are based on the topological descriptions of a large number of experimental studies. They were derived from a broad spectrum of compounds (see Table 1), using charge-density analyses involving different models [*MOLLY* (Hansen & Coppens, 1978), *VALRAY* (Stewart & Spackman, 1983), *LSMOL* (Koritsanszky, 1987) and POP (Craven *et al.*, 1987)] and different diffraction techniques (X-ray only or both X-ray and neutron). This led to 83 hydrogen bonds ($X-H\cdots O$; X = C, N, O), for which $d(H\cdots O)$ distances range from 1.56 to 2.63 Å. Two very strong HBs which involve symmetrical $O-H-O$ interactions [$d(H\cdots O)$ 1.22 and 1.24 Å] are also discussed. The compounds used in this study are listed in Table 1 with name codes, experimental temperatures, models of $\rho(\mathbf{r})$ and methods used [X − X, X − N and X − (X + N)] (Coppens, 1967; Hirshfeld, 1991).

The models involved in the present work are commonly used for electron density studies, and their validity has been extensively tested. Special stress must

ISSN 0108-7681

Table 1. *The compounds used in the topological analysis*

Compound	Code	T (K)	Space group	Model	Method
(*Z*)-*N*-Acetyl-β-dehydrophenylalanine methylamide	ACD	100	*Cc*	*MOLLY*	X − X
N-Acetyl-L-tryptophan methylamide	ACT	103	$P2_12_12_1$	*MOLLY*	X − X
Ammonium dihydrogen phosphate	ADP	158	$I\bar{4}2d$	*MOLLY*	X − (X + N)
Glycyl-L-aspartic acid dihydrate	ASP	123	$P2_12_12_1$	*MOLLY*	X − X
Citrinin	CIT	20	$P2_12_12_1$	*VALRAY*	X − X
Leu-enkephaline trihydrate	ENK	100	$P2_12_12_1$	*MOLLY*	X − X
L-Alanine	LAL	23	$P2_12_12_1$	*VALRAY*	X − X
L-Arginine phosphate monohydrate	LAP	130	$P2_1$	*MOLLY*	X − (X + N)
Lithium bis(tetramethylammonium) hexanitrocobalte(III)	LCO	113	$P\bar{3}$m	*VALRAY*	X − X
L-Dopa	LDO	293	$P2_1$	*LSMOL*l	X − X
1-Methyluracil	MUR	123	*Ibam*	*POP*	X − (X + N)
Methylammonium hydrogen succinate monohydrate	SUC	110	$P2_1/m$	*VALRAY*	X − (X + N)
L-Tyrosyl-glycyl-glycine monohydrate	TGG	123	$P2_12_12_1$	*MOLLY*	X − X
Triglycine	TRG	123	$P\bar{1}$	*MOLLY*	X − X
Urea	URE	123	$P\bar{4}2_1m$	*VALRAY*	X − N

References: ACD: Souhassou *et al.* (1991); ACT: Souhassou *et al.* (1992); ADP: Boukhris (1995), Pérès *et al.* (1999); ASP: Lachekar (1997), Lachekar *et al.* (1999); CIT: Destro & Merati (1993); ENK: Wiest *et al.* (1994); LAL: Destro *et al.* (1988, 1991); LAP: Espinosa *et al.* (1996), Espinosa (1994); LCO: Bianchi *et al.* (1996); LDO: Howard *et al.* (1995); MUR: Klooster *et al.* (1992); SUC: Flensburg *et al.* (1995); TGG: Lachekar (1997); TRG: Pichon-Pesme & Lecomte (1998); URE: Stewart (1991), and referencess therein.

be placed on the information derived from X-ray data only (X − X method) compared with information obtained from both X-ray and neutron data [X − N and X − (X + N) methods]. In the X − X method, the best positions and displacement parameters for all atoms, including H atoms, have been obtained together with the multipolar electron density parameters from X-ray structure factors only (see, for example, Souhassou *et al.*, 1991, 1992). In order to correct the implicit problem of H-atom positions these atoms are constrained (in most cases) at the observed neutron average distances (Allen, 1986; Kvick *et al.*, 1974; Blessing, 1988) in the direction found in the X-ray analysis. However, if we want to obtain the most accurate model of $\rho(\mathbf{r})$, X − N and X − (X + N) methods are, in principle, methodologically better. Both include neutron information before the refinement of the electron density parameters: in the X − N method all atomic positions and displacement parameters are obtained from neutron data and are kept fixed in the multipolar refinement (Coppens, 1967); in the X − (X + N) method only part of the information derived from neutron data (mainly for the H atoms) is included and not refined (Espinosa *et al.*, 1996; Espinosa, 1994). Because thermal diffuse scattering (TDS) and extinction effects are different in X-ray and neutron experiments, the usual problem of the X − N method is the description of thermal smearing, which does not match very well with high-order X-ray results (Blessing, 1995). Often, the Hirshfeld rigid-bond test (Hirshfeld, 1976) applied to neutron results fails where high-order X-ray and multipolar refinements succeed. However, in many cases, a satisfactory description can be derived (Espinosa *et al.*, 1996), especially when it involves positional and displacement parameters describing H atoms only. Thus, it is not surprising to find many more X − (X + N) than X − N studies in the literature. Because the HB geometry (see Fig. 1) and the atomic displacement parameters are not the same whether we introduce neutron information or not, the most significant question is whether, given the actual experimental accuracy and methods, the topological properties and their intrinsic behaviour can be considered equivalent when comparing results from X-ray only or from both X-ray and neutron refinements.

We point out the relevance of the general trends described in this study because of the different experimental conditions, models, refinement strategies and methods. On the other hand, all models use the same mathematical least-squares method to fit pseudoatom electron density parameters; this is sometimes critical because the problem is non-linear and correlations are important in some cases (for instance, between displacement parameters, quadrupoles and scale factors). However, as shown in this paper, the consistency of results from experiments performed in different laboratories at several temperatures (even at room temperature), demonstrates that deconvolution between thermal and electron density parameters is effective with any of the four $\rho(\mathbf{r})$ models presented here (a discussion of the deconvolution problem is given by Moss *et al.*, 1995). Also, the pseudoatom multipolar model may not be the most appropriate for studying $\rho(\mathbf{r})$ in intermolecular regions; the maximum entropy method (MEM) combined with maximum likelihood refinements (Roversi *et al.*, 1998), which estimate the electron density on a fine grid in the unit cell, can reveal important features in intermolecular regions. Furthermore, the phase problem, which is mainly important when non-centrosymmetric space groups are involved, is another implicit source of inaccuracy. Even if the multipolar models of $\rho(\mathbf{r})$ permit a much better description of phases than the spherical-atom model

(Souhassou *et al.*, 1991), the results have to be analysed critically (El Haouzi *et al.*, 1996; Spackman & Byrom, 1997; Pérès *et al.*, 1999): atomic constraints must be applied in some cases and several refinement strategies must be tested to drive the convergence to the most realistic minima. Finally, it is noteworthy that in the intermolecular regions on which this study is focused features in $\rho(\mathbf{r})$ are of much lower magnitude than those around atomic positions, and thus they can be more sensitive to small variations induced by different experiments, methods, models and strategies. On the other hand, the estimated standard uncertainty of the electron density in the intermolecular regions (for instance, in the H···O region) is small because the analysis is performed far from the nuclei (Rees, 1976).

Hydrogen bonding is one of the most interesting features of the electron density of molecular compounds: many molecular materials have crystal periodicity because of HB interactions, which play an important role in chemical and biological properties. HBs are also of importance in changes in physical properties when they are associated with phase transitions. Historically, the initial approach to an HB classification was based on energetics or on geometrical criteria only (such as distances, angles and planes) (Jeffrey & Saenger, 1991). However, the topological characterization of $\rho(\mathbf{r})$ in intermolecular regions now permits a new, accurate, analysis based on quantitative interpretation of the electron density distribution $\rho(\mathbf{r})$, the Laplacian $\nabla^2\rho(\mathbf{r})$ and the principal curvatures $\lambda_1(\mathbf{r})$, $\lambda_2(\mathbf{r})$ and $\lambda_3(\mathbf{r})$ at the (3, −1) critical points (Bader, 1990), as well as on the relevant distances defining the interaction geometry.

In §2 we discuss the position of the critical point (CP) in relation to geometric HB parameters. A discussion concerning neutron data (§3) will then show that current results from joint X-ray and neutron data are equivalent to those calculated from X-ray structure factors alone, given the accuracy attained in both cases. §4 concerns general trends of the topological properties $\rho(\mathbf{r}_{CP})$, $\lambda_3(\mathbf{r}_{CP})$ and $\nabla^2\rho(\mathbf{r}_{CP})$ *versus* characteristic HB distances. Among these topological properties, the relationships found between $\lambda_3(\mathbf{r}_{CP})$ and the characteristic HB distances are especially interesting; they lead to the quantitatively accurate classification of HBs proposed in §5. We also show that the topological properties at the CPs of C—H···O HBs, in spite of the weakness of their interactions, follow a phenomenological behaviour closely analogous to those found for the two stronger types of HBs, N—H···O and O—H···O. As pointed out by a referee, these critical points do also exist (but at different positions) if we calculate the electron density corresponding to a simple superposition of spherical atoms (IAM model), but the values obtained for the principal curvatures are not sensible because the IAM model does not take into account the Pauli principle when an HB interaction is being built (Espinosa *et al.*, 1999).

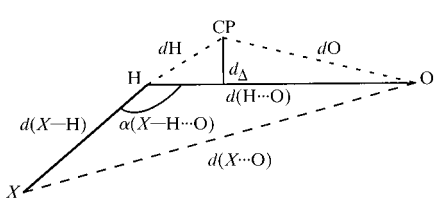

Fig. 1. HB geometry. dH, dO, d(H···O), d(X···O) and α(X—H···O) are the distances from the CP to the H and O atoms, the distances H···O and X···O (X = C, N, O), and the HB angle, respectively.

2. Topological properties of the HB geometry

Table 2 lists the topological properties at the CPs of the HBs used in this study. Most of these topological properties were calculated using the *NEWPROP* program (Souhassou & Blessing, 1999) in which the position of the CP is determined iteratively by

$$\mathbf{r}_{CP} = \mathbf{r}_o + \nabla\rho(\mathbf{r})\mathbf{H}^{-1},$$

where $\mathbf{r}_{CP}$ is the CP position (*i.e.* the point where the gradient of the electron density vanishes), $\mathbf{r}_o$ is a starting point in the iterative search and $\mathbf{H}^{-1}$ is the inverse Hessian matrix. The procedure is stopped when the final gradient value at the CP reaches $\pm 10^{-5}$ e Å^{-4}; the error on the CP position from the iterative process is then estimated to be less than 10^{-3} Å. The highest contribution to the final error in the CP position actually comes from errors in the experimental density parameters, but we estimate the maximum error for all distances involving the CP to be less than 0.02 Å because they do not depend strongly on the nuclear position of H. On the other hand, the experimental s.u.'s associated with the H···O distances in the X—H···O interactions may be as large as $\sigma[d(\text{H}\cdots\text{O})] = 0.05$ Å for X − X experiments. The estimated error in the density at the CP is certainly smaller than 0.05 e Å^{-3} in the intermolecular regions; the estimated errors in the $\lambda(\mathbf{r}_{CP})$'s, and especially in $\nabla^2\rho(\mathbf{r}_{CP})$, are large compared to the distribution of their values for a given X···O or H···O distance (Stewart, 1991, and references therein). Therefore, all data are given without standard uncertainties (s.u.).

Fig. 1 shows the geometry of the HB interaction X—H···O, including the position of the CP associated with that interaction, and the definition of the geometric distances and angles. All HB CPs are of type (3,−1), as expected. The CP position, which lies in the bond path of the HB interaction and which is shared by both H and O basins in the interatomic surface (zero flux surface), is in general slightly out of the H···O direction. Furthermore, no (3,−1) CP has been found between X and O, therefore no direct interaction occurs between X and O.

Table 2. *The topological properties of the 85 HBs (including two symmetrical O—H—O shared-shell interactions) discussed in this study*

The topological distances dH, dO, dH + dO and d(H···O) (Å) are defined in Fig. 1. The electron density ρ (e Å^{-3}), its Laplacian $\nabla^2\rho$(e Å^{-5}) and the curvatures λ_1, λ_2, λ_3 (e Å^{-5}) are the observed values at the (3, −1) CPs of the H···O interactions. In order to identify each HB the notation used in the original paper is kept. Only the topological properties referred in the original papers are given.

Code	O—H···O	dH	dO	dH + dO	d(H···O)	d(X···O)	α(X—H···O)	λ_1	λ_2	λ_3	$\nabla^2\rho$	ρ
LAP	O3—H18···O6	0.50	1.09	1.59	1.589	2.594	172.5	−1.46	−1.40	8.39	5.53	0.30
	O4—H19···O1	0.51	1.08	1.58	1.570	2.560	169.7	−1.76	−1.60	9.66	6.30	0.27
	O*w*—H17···O5	0.62	1.18	1.80	1.793	2.779	172.4	−1.02	−0.95	5.81	3.84	0.19
	O*w*—H16···O5	0.64	1.22	1.86	1.847	2.749	154.0	−0.83	−0.75	4.61	3.03	0.18
ENK	*W*3—H*W*31···O6	0.61	1.20	1.80	1.798	2.773	172.2	−1.25	−1.14	6.55	4.16	0.21
	*W*2—H*W*21···O7	0.63	1.20	1.83	1.824	2.757	162.8	−1.11	−1.04	5.92	3.77	0.19
	*W*1—H*W*11···O4	0.67	1.22	1.88	1.879	2.801	160.5	−0.81	−0.79	5.06	3.46	0.15
	*W*3—H*W*32···O5	0.68	1.22	1.90	1.889	2.799	156.2	−0.81	−0.77	4.84	3.26	0.16
	*W*2—H*W*22···O1	0.71	1.35	2.06	1.926	2.890	173.9	−0.39	−0.18	3.67	3.11	0.10
TGG	O6—H*W*2···O2	0.60	1.20	1.79	1.791	2.752	175.7	−0.97	−0.92	5.69	3.80	0.19
	OH1—HO5···O32	0.54	1.17	1.71	1.705	2.655	167.8	−1.19	−1.17	5.97	3.61	0.21
	O6—H*W*1···O31	0.63	1.23	1.86	1.85	2.800	166.7	−0.83	−0.79	4.86	3.24	0.17
ASP	O*w*2—H*w*21···O21	0.70	1.30	2.00	1.97	2.910	126.3	−0.43	−0.35	3.43	2.65	0.09
	O*w*1—H*w*11···O21	0.56	1.17	1.73	1.731	2.690	172.7	−0.92	−0.92	6.65	4.81	0.20
	O*w*1—H*w*12···O22	0.59	1.18	1.77	1.753	2.696	166.2	−0.97	−0.86	6.05	4.22	0.19
	O*w*2—H*w*22···O*w*1	0.60	1.22	1.82	1.803	2.766	170.9	−0.64	−0.45	5.04	4.21	0.13
	O2D2—HD22···O22	0.53	1.11	1.65	1.643	2.583	165.3	−1.88	−1.76	8.73	5.09	0.31
CIT	O11—HO11···O17		1.09		1.691			−2.12	−1.94	8.51	4.44	0.35
	O18—HO18···O13		1.02		1.561			−3.55	−3.39	11.68	4.74	0.54
LDO	O3—H103···O2	0.65			1.760			−1.34	−1.28	6.52	3.90	0.22
	O4—H104···O4	0.66			1.880			−1.45	−1.05	6.00	3.50	0.20
SUC	O1—H1···O1	0.28	0.94	1.22	1.221	2.442	180.0	−11.99	−11.79	16.97	−6.81	1.06
	O3—H8···O2	0.74	1.11	1.86	1.848	2.796	167.5	−1.22	−1.15	4.61	2.23	0.20
ADP	O—HP···O	0.33	0.91	1.24	1.238	2.474	177.6	−18.24	−15.82	17.04	−17.02	1.30
LAP	N1—H4···O2	0.58	1.18	1.76	1.739	2.772	167.2	−1.07	−0.97	6.28	4.24	0.19
	N1—H3···O2	0.59	1.19	1.78	1.767	2.795	168.8	−0.87	−0.82	6.24	4.55	0.15
	N1—H2···O1	0.62	1.21	1.83	1.815	2.824	161.2	−0.73	−0.82	5.30	3.75	0.17
	N4—H15···O3	0.61	1.23	1.84	1.831	2.845	171.9	−0.68	−0.59	4.83	3.56	0.15
	N4—H14···O*w*	0.65	1.25	1.90	1.883	2.879	166.7	−0.72	−0.58	3.87	2.57	0.14
	N3—H12···O6	0.71	1.29	2.00	1.982	2.922	151.7	−0.46	−0.42	3.14	2.26	0.10
	N2—H11···O6	0.87	1.39	2.26	2.172	3.062	144.0	−0.27	−0.22	1.88	1.39	0.06
ENK	N1—HN13···O6	0.54	1.12	1.66	1.653	2.660	160.9	−1.98	−1.90	9.15	5.27	0.31
	N2—HN2···O7	0.59	1.24	1.83	1.826	2.871	171.1	−0.78	−0.71	6.18	4.69	0.13
	N3—HN3···*W*3	0.74	1.27	2.00	1.941	2.839	140.3	−0.68	−0.64	4.01	2.69	0.13
	N4—HN4···O2	0.70	1.29	1.99	1.941	2.925	156.4	−0.47	−0.41	3.79	2.91	0.09
	N1—HN11···O3	0.71	1.29	2.01	1.987	2.977	154.7	−0.52	−0.51	3.56	2.53	0.11
	N5—HN5···O3	0.79	1.37	2.16	2.079	3.064	155.9	−0.29	−0.23	2.44	1.92	0.06
	N1—HN12···O4	1.07	1.42	2.48	2.385	3.020	118.0	−0.28	−0.22	1.62	1.12	0.08
TGG	N1—HN11···O32	0.57	1.15	1.72	1.718	2.745	172.1	−1.30	−1.24	6.86	4.32	0.25
	N1—HN12···O6	0.62	1.17	1.79	1.773	2.690	145.9	−1.21	−0.98	5.61	3.42	0.22
	N2—HN2···O31	0.62	1.22	1.84	1.838	2.865	174.2	−0.86	−0.83	5.06	3.37	0.17
	N1—HN13···O2	0.68	1.27	1.95	1.922	2.906	158.8	−0.59	−0.48	3.52	2.44	0.13
	N3—HN3···OH1	0.75	1.26	2.01	1.998	2.853	138.7	−0.67	−0.66	3.64	2.31	0.14
TRG	N21— HN21···O13	0.64	1.21	1.85	1.832	2.731	143.4	−1.05	−0.91	5.59	3.63	0.18
	N21—HN23···O24	0.64	1.24	1.88	1.875	2.899	171.6	−1.17	−1.17	4.80	3.96	0.09
	N23—H23···O21	0.71	1.25	1.96	1.941	2.902	153.7	−0.56	−0.54	3.83	2.73	0.12
	N22—H22···O14	0.72	1.29	2.01	1.965	2.909	150.6	−0.53	−0.48	3.74	2.73	0.11
	N12—H12···O12	0.76	1.31	2.07	2.005	2.960	101.0	−0.29	−0.25	2.86	2.20	0.07
	N13—H13···O22	0.81	1.34	2.15	2.136	3.075	150.5	−0.34	−0.33	4.37	1.69	0.08
	N21—HN22···O13	1.16	1.51	2.67	2.608	2.731	140.2	−0.18	−0.14	1.16	0.84	0.05
	N11—HN12···O23	0.60	1.15	1.75	1.745	2.724	156.7	−1.26	−1.15	6.57	4.17	0.21
	N11—HN11···O23	0.74	1.14	1.88	1.883	2.909	171.5	−1.15	−1.13	4.72	2.44	0.25
	N11—HN13···O23	0.60	1.15	1.75	1.750	2.776	173.1	−1.39	−1.35	6.75	4.01	0.24
ASP	N1—HN13···O21	0.61	1.28	1.89	1.881	2.885	168.4	−0.46	−0.41	3.80	2.93	0.12
	N2—HN2···O1	0.71	1.32	2.03	1.957	2.987	169.7	−0.23	−0.17	3.00	2.60	0.05
	N1—HN11···O*w*1	0.67	1.26	1.93	1.890	2.811	145.1	−0.92	−0.73	4.23	2.58	0.18
	N1—HN12···O*w*2	0.63	1.21	1.84	1.822	2.759	149.3	−0.90	−0.75	4.77	3.12	0.17
LAL	N—H1···O1		1.16		1.827	2.835	161.0	−1.10	−1.10	5.70	3.50	0.19
	N—H2···O2		1.16		1.832	2.814	161.2	−1.20	−1.20	6.00	3.60	0.20
	N—H3···O2		1.11		1.722	2.792	169.5	−1.70	−1.70	8.10	4.70	0.27
LDO	N1—H2N···O1	0.63			1.960			−0.71	−0.64	4.01	2.65	0.15

Table 2 (*cont.*)

Code	O—H···O	*d*H	*d*O	*d*H + *d*O	*d*(H···O)	*d*(*X*···O)	α(*X*—H···O)	λ_1	λ_2	λ_3	$\nabla^2\rho$	ρ
	N1—H3N···O1	0.62			1.940			−0.92	−0.89	4.72	2.91	0.19
	N1—H1N···O2	0.64			1.830			−1.26	−1.25	6.15	3.64	0.24
SUC	N1—H4···O2	0.66	1.20	1.86	1.858	2.866	164.9	−1.40	−1.30	4.56	1.86	0.22
	N1—H5···O3	0.58	1.15	1.73	1.725	2.763	178.1	−1.99	−1.91	6.36	2.46	0.29
ACD	N1—H01···O1	0.66	1.16	1.81	1.814	2.835	170.5	−1.32	−1.24	6.14	3.58	0.22
	N2—H02···O2	0.69	1.17	1.85	1.849	2.869	170.3	−1.09	−1.06	5.48	3.33	0.19
ACT	N1—H01···O2	0.75	1.23	1.98	1.979	3.010	173.9	−0.68	−0.67	3.51	2.15	0.15
	N2—H02···O1	0.70	1.22	1.92	1.918	2.880	155.0	−1.05	−0.99	4.11	2.06	0.21
	N3—H03···O1	0.67	1.19	1.86	1.863	2.890	172.1	−1.20	−1.04	4.55	2.31	0.22
ADP	N—Hs···O	0.75	1.20	1.95	1.940	2.889	156.8	−1.10	−0.98	4.21	2.12	0.22
	N—Hl···O	1.09	1.56	2.64	2.634	3.172	89.2	−0.14	−0.12	0.95	0.69	0.04
URE	N—H2···O	0.80	1.35	2.15	2.067	2.960	147.6				1.54	0.08
	N—H1···O	0.69	1.33	2.02	2.009	2.998	166.8				2.32	0.06
MUR	N3—H3···O4				1.770			−1.90	−1.70	5.70	2.10	0.23
TRG	C2A1—H211···O14	0.84	1.39	2.23	2.219	3.161	144.0	−0.40	−0.37	2.33	1.56	0.10
	C2A2—H221···O21	1.10	1.38	2.48	2.463	3.136	119.0	−0.24	−0.22	1.52	1.06	0.07
	C1A1—H111···O12	1.18	1.42	2.60	2.529	3.016	106.1	−0.25	−0.15	1.41	1.01	0.07
	C1A2—H122···O22	1.11	1.45	2.56	2.540	3.190	116.2	−0.20	−0.17	1.22	0.85	0.06
LCO	C1—H11···O1	1.15			2.583	3.607	156.7	−0.04	−0.01	0.41	0.36	0.02
	C1—H12···O2	1.11			2.519	3.251	124.4	−0.16	−0.15	1.08	0.77	0.05
	C2—H21···O1	1.10			2.498	3.543	169.7	−0.21	−0.05	0.86	0.66	0.04
	C2—H21···O2	1.16			2.591	3.476	140.9	−0.17	−0.08	0.84	0.59	0.03
MUR	C6—H6···O2				2.370			−0.40	−0.30	1.90	1.10	0.07
	C1—H11···O4				2.340			−0.40	−0.30	1.30	0.60	0.06

The distance d_Δ between the CP and the H···O direction is given by

$$d_\Delta = \big(d^2\mathrm{H} - \{[d^2(\mathrm{H}\cdots\mathrm{O}) + d^2\mathrm{H} - d^2\mathrm{O}]/ \times 2d(\mathrm{H}\cdots\mathrm{O})\}^2\big)^{1/2},$$

where *d*H and *d*O are the distances from H and O to the CP, respectively. The deviation d_Δ ranges from 0.00 to 0.12 Å for all HBs referenced in this work.

Bearing in mind the s.u.'s of the distances (as discussed above), inspection of Figs. 2(*a*), 2(*b*) and 2(*c*), which show plots of *d*H, *d*O and *d*H + *d*O *versus* the intermolecular distance *d*(H···O), reveals a global linear relationship. The excellent linear fit obtained in Fig. 2(*c*) is a consequence of the general relationship

$$d^2(\mathrm{H}\cdots\mathrm{O}) = d^2\mathrm{H} + d^2\mathrm{O} + 2\mathbf{dH}.\mathbf{dO}$$

with cos(**dH**, **dO**) close to unity, because the slope is not significantly different from unity, as indicated by the s.u.'s on the regression parameters. This fact is related to the very small d_Δ values and to the projection of the CP on the H···O direction, which lies within 0.50–1.18 Å from the H-atom position. Thus, as the estimate of the error of any distance involving the CP position is not better than 0.02 Å, we conclude that, for most of the observed HBs, the bond path lies on the H···O direction within experimental accuracy.

On the other hand, in spite of the intrinsic problem of the H-atom positions, the fit for Fig. 2(*a*) involving X-ray data only is very good (correlation factor = 0.98), supporting the validity of using this type of information (see §3). It is also surprising that the dispersion of points around the linear fit of Fig. 2(*a*) (involving H-atom positions) is smaller than that found in Fig. 2(*b*) (involving O-atom positions). The larger dispersions found in Figs. 2(*a*) and 2(*b*) compensate each other in Fig. 2(*c*).

We point out that the observed range of *d*H distances (approximately 0.50–1.18 Å) is larger than that found for *d*O distances (approximately 1.02–1.56 Å), leading to the conclusion that the topological radius of the H atom in the H···O HB direction changes more than that of the O atom. The CP position determines the bonded radius (*d*H and *d*O) in the HB direction, and so it should be correlated with the respective atomic volumes and their related properties (such as, for instance, polarizability).

3. Is it necessary to use only combined X-ray and neutron data in this study?

In order to decide whether it is necessary to use H-atom positions and displacement parameters obtained from neutron diffraction, we analysed the topological properties of $\rho(\mathbf{r})$ calculated by the X − X method, and by the X − N and X − (X + N) methods. To do this we plotted the electron density $\rho(\mathbf{r}_{CP})$ (Fig. 3), the Laplacian of the electron density $\nabla^2\rho(\mathbf{r}_{CP})$ (Fig. 4) and the positive curvature $\lambda_3(\mathbf{r}_{CP})$ (Fig. 5) observed at the HB CPs, against the topological *d*H, *d*O and *d*(H···O) distances. In all cases we have fitted simple exponential curves: the continuous lines show the fit for data from X − X refinements only and the dotted lines show the corresponding fit for data from X − N and X − (X + N) refinements. In this section these curves must be thought

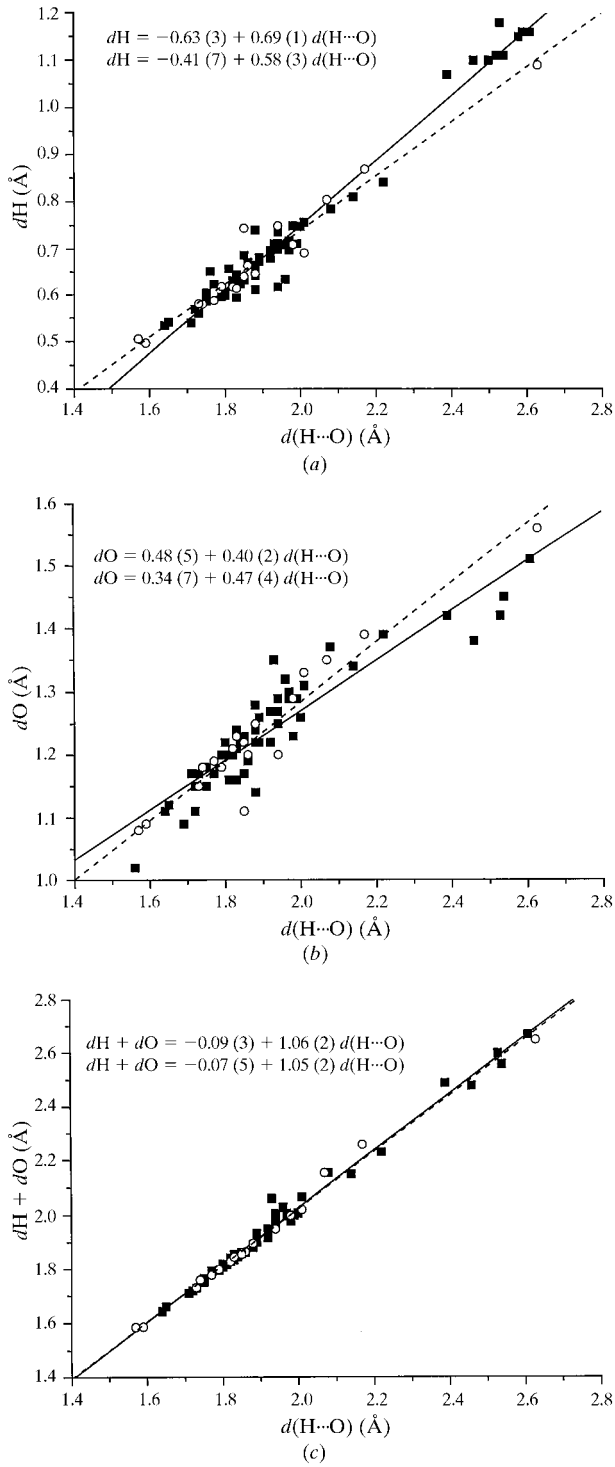

Fig. 2. Phenomenological behaviour of $d(H\cdots O)$ *versus* (*a*) dH, (*b*) dO and (*c*) dH + dO. The two fitted curves in each graph are for X-ray data only (line and first equation) and joint X-ray and neutron data (dashed line and second equation). Points represented by filled squares and empty circles are derived from X-ray data only and joint X-ray and neutron data, respectively. The correlation factors R are 0.98 and 0.97, 0.92 and 0.96, and 0.99 and 1.00, for the first and second equations in (*a*), (*b*) and (*c*), respectively.

of as visual guides, because we are more interested in the distribution of the points around the curves rather than in the fits themselves.

As shown in Figs. 3, 4 and 5, the topological values $\rho(\mathbf{r}_{CP})$, $\nabla^2\rho(\mathbf{r}_{CP})$ and $\lambda_3(\mathbf{r}_{CP})$, obtained either from X-ray data only or from joint X-ray and neutron data, are similar when compared over the observed range of distances. In particular, the fits of $\lambda_3(\mathbf{r}_{CP})$ *versus* dH, dO and $d(H\cdots O)$ for X-ray data only and for joint X-ray and neutron data lead to the same phenomenological behaviour. Therefore, we cannot distinguish between results from X − X, X − N or X − (X + N) data. In this way, the implicit neutron information introduced in the X − X method, by means of the average distances (O—H, N—H and C—H) observed from neutron experiments (Allen, 1986), is presently good enough to describe the topological properties [$\rho(\mathbf{r}_{CP})$, $\nabla^2\rho(\mathbf{r}_{CP})$ and $\lambda_3(\mathbf{r}_{CP})$] when compared with those obtained from X − N and X − (X + N) methods. In conclusion, with the present accuracy of measurements and corrections, results from X-ray data only or from both X-ray and neutron data are essentially equivalent and therefore may be used in this study.

4. Behaviour of $\rho(\mathbf{r}_{CP})$, $\nabla^2\rho(\mathbf{r}_{CP})$ and $\lambda_3(\mathbf{r}_{CP})$ *versus* characteristic distances

We recall that this study concerns a broad spectrum of HBs (O—H···O, N—H···O and C—H···O). Inspection of all plots concerning the positive curvature $\lambda_3(\mathbf{r}_{CP})$ (Fig. 5), as well as the plots of $\rho(\mathbf{r}_{CP})$ *versus* dO (Fig. 3*b*) and $\nabla^2\rho(\mathbf{r}_{CP})$ *versus* dH (Fig. 4*a*), show exponential behaviour with a narrow spread of points. The correlation between the positive curvature $\lambda_3(\mathbf{r}_{CP})$ and the topological distances is especially excellent. Only one point far away from the fitting curves in most plots has been detected; this concerns one HB in TRG. Because $\nabla^2\rho$ is the sum of the three principal curvatures, the dispersions found in the Laplacian plots are larger than those found in the λ_3 plots. The most important result of this study concerns the exponential behaviour of $\lambda_3(\mathbf{r}_{CP})$ as a function of $d(H\cdots O)$ (Fig. 5): the dispersion of the data is very small, leading to quantitative agreement.

5. A classification of HBs based on $\lambda_3(\mathbf{r}_{CP})$

Topological analysis of the electron density is one of the most powerful tools for classifying HB interactions. To demonstrate a tentative classification, Table 3 shows the topological properties at the CP of some pure covalent (H_2, B_2, N_2, O_2) and ionic (LiCl, NaCl, NaF, KF) interactions (Bader, 1990), as well as those of the X—H (X = C, N, O) covalent bonds in LAP (Espinosa *et al.*, 1996). In the topological analysis of $\rho(\mathbf{r})$, Bader (1990) classifies covalent and ionic interactions as shared and closed-

shell interactions, respectively. The fundamental difference is the sign of $\nabla^2\rho(\mathbf{r}_{CP})$, which is related to a local concentration [shared interactions: $\nabla^2\rho(\mathbf{r}_{CP}) < 0$ and a large $\rho(\mathbf{r}_{CP})$ value] or dilution [closed-shell interactions: $\nabla^2\rho(\mathbf{r}_{CP}) > 0$ and a small $\rho(\mathbf{r}_{CP})$ value] of the electron density at the CP, respectively. Initially, HBs were

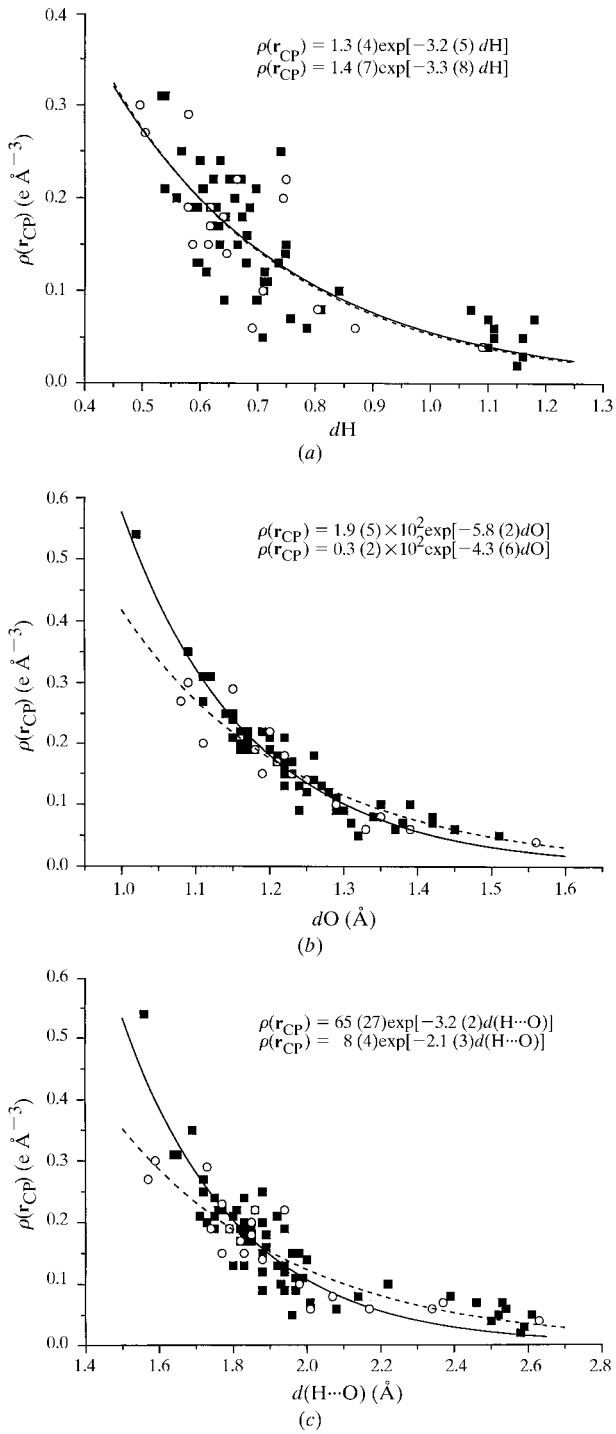

Fig. 3. Phenomenological behaviour of $\rho(\mathbf{r}_{CP})$ *versus* (*a*) *d*H, (*b*) *d*O and (*c*) *d*(H···O). Curves, equations and data points are defined as in Fig. 2. The chi-squared values ($\times 10^{-3}$) are 1.9 and 2.6, 0.5 and 1.1, and 1.6 and 1.5 for the first and second equations in (*a*), (*b*) and (*c*), respectively.

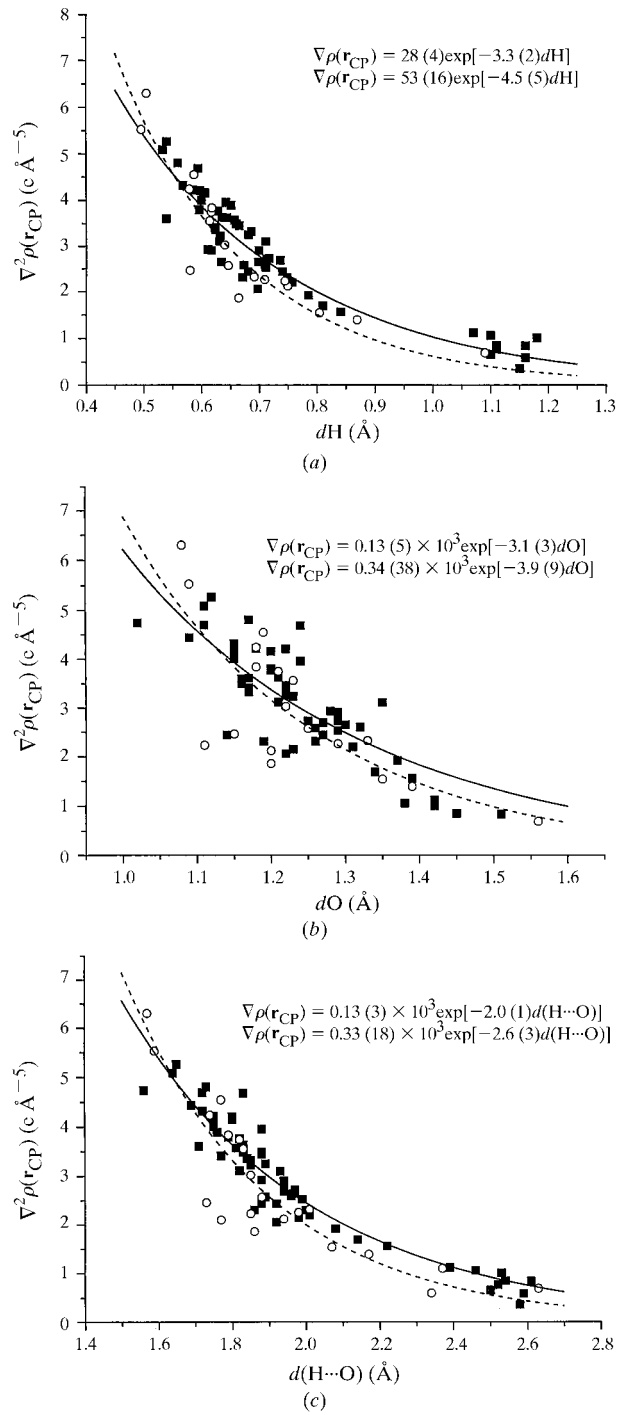

Fig. 4. Phenomenological behaviour of $\nabla^2\rho(\mathbf{r}_{CP})$ *versus* (*a*) *d*H, (*b*) *d*O and (*c*) *d*(H···O). Curves, equations and data points are defined as in Fig. 2. The chi-squared values ($\times 10^{-1}$) are 1.7 and 3.2, 4.3 and 9.7, and 1.6 and 4.4 for the first and second equations in (*a*), (*b*) and (*c*), respectively.

Table 3. *Topological properties at the CP of some pure covalent (H_2, B_2, N_2, O_2) and some pure ionic (LiCl, NaCl, NaF, KF) interatomic interactions (Bader, 1990), as well as the X—H (X = C, N, O) covalent bonds observed in LAP (Espinosa et al., 1996; Espinosa, 1994), two symmetrical O—H—O interactions (Boukhris, 1995; Flensburg et al., 1995) and the H···O HBs used in this study*

For the *X*—H, O—H—O and O···H interactions the first and second rows represent the maximum and the minimum magnitudes of each topological property at the CP, respectively.

Interaction		$\lambda_1(\mathbf{r}_{CP})$	$\lambda_2(\mathbf{r}_{CP})$	$\lambda_3(\mathbf{r}_{CP})$	$\nabla^2\rho(\mathbf{r}_{CP})$	$\rho(\mathbf{r}_{CP})$
Shared	H_2	−23.9	−23.9	14.6	−33.2	1.84
	B_2	−2.4	−2.4	0.0	−4.8	0.84
	N_2	−46.6	−46.6	19.7	−73.5	4.87
	O_2	−35.5	−35.5	46.6	−24.4	3.72
	C—H	−17.4	−16.5	18.4	−16.9	1.83
		−15.1	−14.3	14.6	−12.4	1.65
	N—H	−29.8	−27.9	31.5	−28.0	2.25
		−24.2	−24.1	27.8	−18.2	1.97
	O*w*—H	−34.8	−34.4	38.4	−30.8	2.30
		−29.8	−29.0	35.2	−23.6	2.12
	O(P)—H	−27.9	−27.5	32.7	−22.7	1.99
		−26.7	−26.1	30.8	−22.0	1.97
	HB: O—H—O	−18.2	−15.8	17.0	−17.0	1.30
		−12.0	−11.8	17.0	−6.8	1.06
Closed shell	HB: O···H	−3.6	−3.4	11.7	6.3	0.54
		−0.04	−0.01	0.4	0.4	0.02
	LiCl	−1.8	−1.8	9.9	6.3	0.31
	NaCl	−1.0	−1.0	6.8	4.8	0.24
	NaF	−2.2	−2.2	15.5	11.1	0.37
	KF	−1.7	−1.7	11.0	7.6	0.37

considered as closed-shell interactions, because they showed $\nabla^2\rho(\mathbf{r}_{CP}) > 0$. However, recent topological analyses involving symmetrical O—H—O interactions (Boukhris, 1995; Flensburg *et al.*, 1995) (also given in Table 3) are characterized by $\nabla^2\rho(\mathbf{r}_{CP}) < 0$. Thus, topological analysis shows that HBs can cover the spectrum of bonding interactions, from closed to shared-shell, a transition that parallels the shortening and strengthening of the HBs.

It is difficult to classify the degree of covalency and ionicity of several interatomic interactions unambiguously when chemically different atoms are involved. It is well known that a classification based only on $\rho(\mathbf{r}_{CP})$ values is not valid if we compare interactions involving different types of atoms because it depends on their electronic configurations: in Table 3, for covalent interactions, the magnitude of $\rho(\mathbf{r}_{CP})$ ranges from 0.84 e Å^{-3} (for B_2) to 4.87 e Å^{-3} (for N_2); moreover, the magnitude of $\rho(\mathbf{r}_{CP})$ in the pure σ covalent bond in H_2 is smaller than that observed for other σ covalent bonds *X*—H, because *X* contributes at the CP with a more populated valence shell than H. On the other hand, we find the same problem if we evaluate the ionicity of an HB interaction as a function of $\rho(\mathbf{r}_{CP})$: on average, Table 3 shows that the $\rho(\mathbf{r}_{CP})$ values found in H···O HBs are smaller than those observed in pure ionic interactions.

The most objective criterion for the classification of HBs is to compare the topological properties induced by both H and O atoms at the CP when they are involved in different interactions. Because this method permits us to quantify interactions in terms of all of the important characteristics of the electron density, we prefer to use the concepts of shared and closed-shell rather than the qualitative covalent/ionic partial character when referring to HBs. For the bonds classified as shared interactions in Table 3, all topological magnitudes $\lambda_1(\mathbf{r}_{CP})$, $\lambda_2(\mathbf{r}_{CP})$, $\lambda_3(\mathbf{r}_{CP})$, $\nabla^2\rho(\mathbf{r}_{CP})$ and $\rho(\mathbf{r}_{CP})$ decrease from O*w*—H to O—H—O unambiguously (the observed ranges between the maxima and the minima of each O—H interaction do not intersect). This observation also holds for the O···H closed-shell interactions. Thus, $\rho(\mathbf{r}_{CP})$ and $\nabla^2\rho(\mathbf{r}_{CP})$ can be used to assign a degree of sharing to any interaction involving both H and O atoms, and permit the general classification given in Table 3: O*w*—H, O(P)—H, then O—H—O and finally O···H, which are also ordered from shorter to longer distances. However, inside each of these groups a conclusive classification based on the experimental topological properties $\rho(\mathbf{r}_{CP})$ and $\nabla^2\rho(\mathbf{r}_{CP})$ cannot be performed unambiguously, in particular for O···H closed-shell interactions. On the contrary, the positive curvature $\lambda_3(\mathbf{r}_{CP})$, which is related to the overlap between the electron clouds of both H and O atoms, shows a very well defined behaviour *versus* d(H···O) in all *X*—H···O interactions. Hence, λ_3 represents the tightening created in the topological distribution of $\rho(\mathbf{r})$ around the CP towards the atomic basins in their closed-shell interaction because λ_3 is proportional to the kinetic energy density at the critical point G^{CP}, reflecting the Pauli principle (Espinosa *et al.*, 1998, 1999). Therefore,

among all topological properties the positive curvature $\lambda_3(\mathbf{r}_{CP})$ is the best candidate for the characterization and classification of HB interactions.

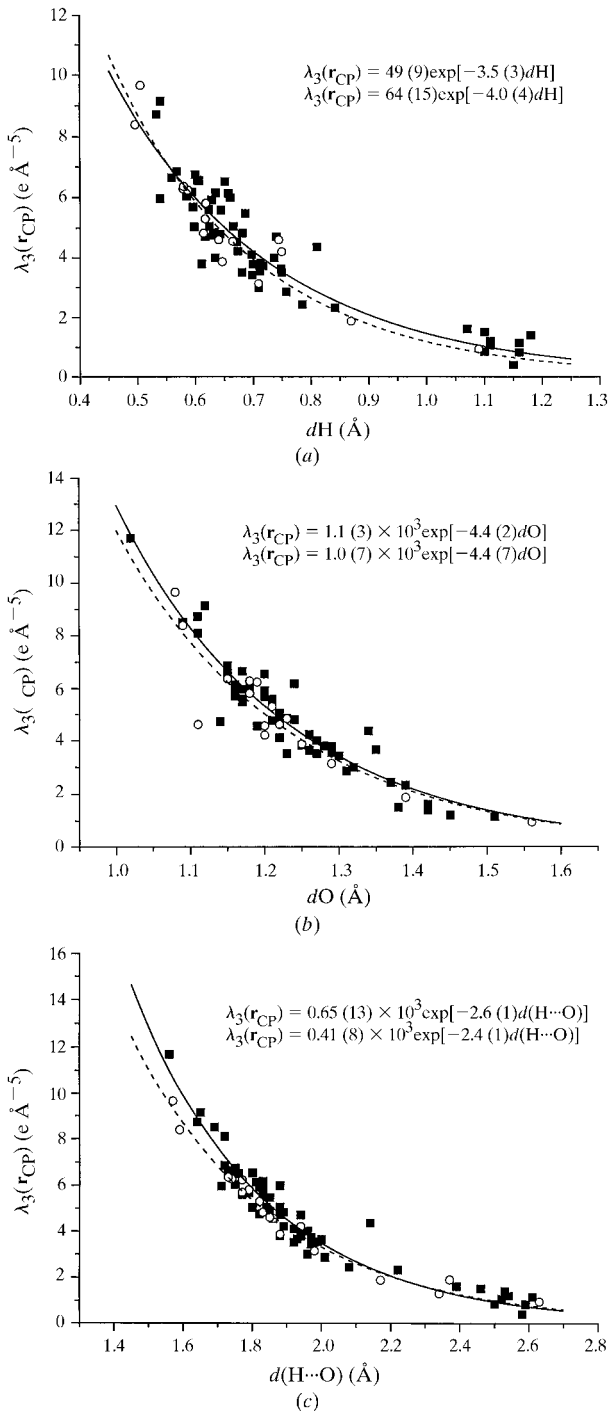

Fig. 5. Phenomenological behaviour of $\lambda_3(\mathbf{r}_{CP})$ *versus* (*a*) *d*H, (*b*) *d*O and (*c*) d(H···O). Curves, equations and data points defined as in Fig. 2. The chi-squared values ($\times 10^{-1}$) are 6.1 and 4.6, 4.7 and 9.1, and 3.4 and 1.1 for the first and second equations in (*a*), (*b*) and (*c*), respectively.

6. Conclusions

This paper describes a new attempt to characterize the topological features of the electron density of hydrogen bonding derived from high-resolution X-ray experiments. The positive curvature at the critical point, $\lambda_3(\mathbf{r}_{CP})$, is the most meaningful parameter for the characterization and classification of HBs, because it shows a very well defined behaviour *versus* all pertinent geometrical and energetic HB parameters [*d*H, *d*O and d(H···O); G^{CP}] and is a good representation when closed-shell interactions are involved.

This work was supported by the University Henri Poincaré (UHP) Nancy 1, the CNRS (UPRESA 7036) and the PB93–0119 project from Dirección General de Investigación Científica y Técnica (DGICYT). EE is grateful to UHP for a six-month invited Maître de Conferences position in Nancy. We are also very grateful to Professor R. F. Bader for helpful comments during his stay as Visiting Professor in Nancy.

References

Abramov, Yu. A. (1997). *Acta Cryst.* A**53**, 264–272.
Allen, F. H. (1986). *Acta Cryst.* B**42**, 515–522.
Bader, R. F. W. (1990). *Atoms in Molecules: a Quantum Theory*. The International Series of Monographs in Chemistry. Oxford: Clarendon Press.
Bianchi, R., Gatti, C., Adovasio, V. & Nardelli, M. (1996). *Acta Cryst.* B**52**, 471–478.
Blessing, R. H. (1988). *Acta Cryst.* B**44**, 334–340.
Blessing, R. H. (1995). *Acta Cryst.* B**51**, 816–823.
Boukhris, A. (1995). Thèse de Doctorat d'Etat, University of Agadir, Morocco, and Henri Poincaré, France.
Coppens, P. (1967). *Science*, **158**, 1577–1579.
Craven, B. M., Weber, H. P. & He, X. M. (1987). *The POP Least-Squares Refinement Procedure*. Technical Report Department of Crystallography, University of Pittsburgh, USA.
Destro, R., Bianchi, R., Gatti, C. & Merati, F. (1991). *Chem. Phys. Lett.* **186**, 47–52.
Destro, R., Marsh, R. E. & Bianchi, R. (1988). *J. Phys. Chem.* **92**, 966–973.
Destro, R. & Merati, F. Z. (1993). *Z. Naturforsch. Teil A*, **48**, 99–104.
Dovesi, R., Saunders, V. R. & Roetti, C. (1995). *CRYSTAL*95 – *An Ab Initio Hartree-Fock LCAO Program for Periodic Systems*. User Manual. University of Turino, Italy.
El Haouzi, A., Hansen, N. K., Le Hénaff, C. & Protas, J. (1996). *Acta Cryst.* A**52**, 291–301.
Espinosa, E. (1994). PhD Thesis, University of Barcelona, Spain.
Espinosa, E., Lecomte, C. & Molins, E. (1999). *Chem. Phys. Lett.* **300**, 745–748.
Espinosa, E., Lecomte, C., Molins, E., Veintemillas, S., Cousson, A. & Paulus, W. (1996). *Acta Cryst.* B**52**, 519–534.
Espinosa, E., Molins, E. & Lecomte, C. (1998). *Chem. Phys. Lett.* **285**, 170–173.

Flensburg, C., Larsen, S. & Stewart, R. F. (1995). *J. Phys. Chem.* **99**, 10130–10141.
Gatti, C., Saunders, V. R. & Roeti, C. (1994). *J. Chem. Phys.* **101**, 10686–10696.
Hansen, N. K. & Coppens, P. (1978). *Acta Cryst.* A**34**, 909–921.
Hirshfeld, F. L. (1976). *Acta Cryst.* A**32**, 239–244.
Hirshfeld, F. L. (1991). *Crystallogr. Rev.* **2**, 169–204.
Howard, S. T., Hursthouse, M. B., Lehmann, C. W. & Poyner, E. A. (1995). *Acta Cryst.* B**51**, 328–337.
Jeffrey, G. A. & Saenger, W. (1991). *Hydrogen Bonding in Biological Structures*. New York: Springer–Verlag.
Klooster, W. T., Swaminathan, S., Nanni, R. & Craven, B. M. (1992). *Acta Cryst.* B**48**, 217–227.
Koritsanszky, T. (1987). *LSMOL Program*. SUNY Buffalo, NY, USA.
Kvick, A., Koetzle, T. F. & Thomas, J. (1974). *J. Chem. Phys.* **61**, 2711–2717.
Lachekar, H. (1997). Thèse de l'Université Henri Poincaré, Nancy 1, France.
Lachekar, H., Pichon-Pesme, V., Souhassou, M. & Lecomte, C. (1999). In preparation.
Moss, G. R., Souhassou, M., Blessing, R. H., Espinosa, E. & Lecomte, C. (1995). *Acta Cryst.* B**51**, 650–660.
Pérès, N., Boukhris, A., Souhassou, M., Gavoille, G. & Lecomte, C. (1999). *Acta Cryst.* A**55**. In the press.
Pichon-Pesme, V. & Lecomte, C. (1998). *Acta Cryst.* B**54**, 485–493.
Platts, J. A. & Howard, S. T. (1996). *J. Chem. Phys.* **105**, 4668–4674.
Rees, B. (1976). *Acta Cryst.* A**32**, 483–488.
Roversi, P., Irwin, J. J. & Bricogne, G. (1998), *Acta Cryst.* A**54**, 971–996.
Souhassou, M. & Blessing, R. H. (1999). *J. Appl. Cryst.* **32**, 210–217.
Souhassou, M., Lecomte, C., Blessing, R. H., Aubry, A., Rohmer, M.-M., Wiest, R., Bénard, M. & Marraud, M. (1991). *Acta Cryst.* B**47**, 253–266.
Souhassou, M., Lecomte, C., Ghermani, N.-E., Rohmer, M.-M., Wiest, R., Bénard, M. & Blessing, R. H. (1992). *J. Am. Chem. Soc.* **114**, 2371–2382.
Spackman, M. A. & Byrom, P. G. (1997). *Acta Cryst.* B**53**, 553–564.
Stewart, R. F. (1991). In *The Application of Charge Density Research to Chemistry and Drug Design*. NATO ASI Series, Physics, Vol. 250, edited by G. A. Jeffrey and J. F. Piniella. New York: Plenum Press.
Stewart, R. F. & Spackman, M. A. (1983). *VALRAY User's Manual*. Department of Chemistry, Carnegie-Mellon University, Pittsburgh, USA.
Wiest, R., Pichon-Pesme, V., Bénard, M. & Lecomte, C. (1994). *J. Phys. Chem.* **98**, 1351–1362.